Review

Electron Spectroscopy of Charge Exchange Effects in Low Energy Ion Scattering at Surfaces: Case Studies of Heavy Ions at Al Surface

Pierfrancesco Riccardi (ID)

Dipartimento di Fisica and INFN Gruppo collegato di Cosenza, Università della Calabria, Via P. Bucci cubo 33c, 87036 Rende, CS, Italy; pierfrancesco.riccardi@unical.it

Abstract: This work discusses studies of electron emissions during the interaction of low energy (in the keV energy range and below) singly charged ions with Aluminum surfaces. Analysis of the spectra provides insight into the electronic excitation processes and the dynamics of the interaction of the projectiles with the surface excitation. The work is primarily focused on the clarification of the role of electron promotion in charge exchange processes that occur during the cascade of atomic collisions. The work highlights the importance of the solid environment and of electron correlation in the understanding of charge exchange and energy deposition in ion-solids interactions.

Keywords: surface scattering; autoionization and auger processes; ion beam analysis; electron emission

1. Introduction

Electronic interactions and charge exchange during the scattering of atomic particles at solid surfaces are important in many areas of both basic and applied research, such as spectroscopy and microscopy of surfaces, plasma discharge, astrophysics, particle accelerators, and medical research. Charge exchange processes include both local and non-local interactions with the surface. Non-local interactions occur at distance from the surface in both the incoming and the outgoing trajectory. The pioneering work of Hagstrum [1–4] provided the foundations of the basic understanding of non-local charge exchange in terms of resonant and Auger (or Auger–Meitner, following a recent proposal [5]) electron capture processes [1–4,6–8] that involve the electronic structure of the solid surface. The sudden creation of a hole in the valence band upon neutralization of incoming ions can lead to plasmon excitation, a third mechanism [9–12] that has been investigated for free electron Al and Mg metal surfaces. On the other hand, local interactions occur during close encounters between atomic particles. Excitations during atomic collisions in solids are satisfactorily described in terms of a molecular orbital (MO) electron promotion model [13–17], such as collisions in the gas phase. In this model, the collisional system is described as a transient quasimolecule in which some molecular orbitals increase their energy as the internuclear distance decreases. Under non-adiabatic conditions [13,14], electrons in these MOs can be transferred (electron promotion) to higher-lying empty Mos at the expense of the kinetic energy of the projectile. After the collision, one or both atoms can be found in excited states that can be revealed by the associated projectile's energy loss or when they decay via electron or photon emission.

The concurrence of several local and non-local processes makes the understanding of the charge, excitation state, and energy loss of scattered particles a very complex issue, which is often addressed, considering the scattering, as a three-step process, that includes non-local charge exchange in the incoming trajectory, a local binary atomic collision, and, finally, further charge exchange in the outgoing trajectory of the scattered projectiles. This picture is further complicated by secondary effects, such as the electronic and atomic collision cascade, meaning a detailed description of several charge exchange mechanisms

has not yet been achieved, resulting in some confusion in the literature. As mentioned above, electron emission is one of the outcomes of these processes that can provide information into the electronic excitation processes and the dynamics of the interaction of the projectiles with the surface [6,7]. Very recently, our group used electron spectroscopy to study the charge exchange phenomena that occur during the binary collisions suffered by the incoming particles and the recoiling target atoms. These processes are currently the subject of intense investigations [18–31] due to their crucial importance in determining the charge and excitation states of scattered projectiles and their energy losses. With the purpose of providing basic insight into charge exchange effects and to discuss these effects within the context of the most recent research on low-energy ion scattering at surfaces, this paper reviews studies of electron emission during the interaction of low energy (in the keV energy range and below) singly charged ions with Aluminum surfaces. Aluminum has been extensively used in studies of ion scattering because it is a prototypical free electron metal. Nevertheless, mechanisms for local charge exchange in the scattering of slow ions at Al surfaces have not yet been identified or clarified and represent an interesting problem that will be addressed in this work. Moreover, the results apply to other substrates, such as Si films, where charge exchange processes have been found to be an important process for energy loss and energy deposition of heavy ions [18–20]. The use of electron spectroscopy allows for the identification of specific charge exchange processes occurring during ion-surface interactions and correlates these process with measured electron emission yields. The goal is to clarify the role of electron promotion in charge exchange processes that occur during the cascade of atomic collisions. This is relevant to current research on charge fraction from surfaces [21,22,25] as well as on energy loss in Si films [18–20]. More generally, the basic understanding of the processes investigated in this work is relevant to many applications in which ion scattering and electron emission are fundamental processes, such as techniques of spectroscopy and microscopy of surfaces, gas discharge, and in research on energy deposition in solids.

The work is organized as follows. In the next chapter, a general overview of the basic mechanisms for electron emission is provided, classified in the two main classes of potential electron emission (PEE) and kinetic electron emission (KEE), depending on whether electrons are excited by the transfer of the potential or the kinetic energy carried by the incoming projectiles. Chapters three and four provide a brief overview of the experimental technique and a presentation of the primary experimental results. Finally, a discussion of the experimental results is provided, which is primarily focused on the clarification of the role of electron promotion in determining electron excitations and the excitation and charge states of scattered projectiles during collision of low energy ions with an Aluminum surface.

2. Mechanisms for Electron Emission

Ion-induced electron emission from solids is historically categorized into two main classes of potential and kinetic electron emission [6,7]. In potential electron emission (PEE), the source of electronic excitation is the potential energy carried by incoming particles because of their excitation/ionization state. As discussed above, this potential energy is converted into electronic excitation when the incoming particle is neutralized or deexcited by electron capture by the surfaces, leading to electron emission via Auger processes or plasmon excitation and decay. PEE dominates the emission at low impact energy; when impact energies are increased, electron emission becomes dominated by the transfer of the kinetic energy of incoming particles (kinetic electron emission, or KEE).

2.1. PEE

The basic method for studying the potential emission of electrons was developed by Hagstrum in the 1950s and has been extensively reviewed [1–4]. Hagstrum treated these processes as Auger transitions between the solid and a projectile carrying potential energy

by virtue of its state of excitation and/or ionization. The idea is that an Auger transition occurs before the projectile penetrates the solid, neutralizing the hole, and emitting an electron into the vacuum. If one of the two electrons participating in the Auger process belongs to the projectile and the other to the solid, we speak of Auger de-excitation (AD). Since the electrons in the solid can come from any level of the valence band, the AD process produces excited electrons in an energy range of width W, where W is the width of the band. The electronic spectra of the electrons emitted following AD processes reflect the density of the states of the target surface (modified by the field of the incident ion) weighted by a transition probability that depends on the energy and symmetry of the electronic states involved [1,7].

If the projectile is an ion, it can be neutralized by an interatomic Auger process in which the two electrons belong to the solid. This process is called Auger Neutralization (AN). Since this process involves two electrons of the solid, the spectrum of the emitted electrons will have an amplitude approximately equal to 2 W.

Another mechanism of PEE involves the excitations and the subsequent decay of plasmons [9–12]. Plasmons of energy E_{pl} can be excited if $E_n > E_{pl}$. The process excites surface plasmons, most likely multipole plasmons [32]. Their subsequent decay by the excitation of valence electrons (interband transitions) may result in the emission of electrons that produce a characteristic structure in the electron energy distribution [9,11,12,32].

Figure 1 schematically illustrates the mentioned processes. Also shown are those processes that do not result directly in electron emission, like the resonant charge transfer processes. Resonant neutralization does not give rise to electron emission directly, but it is very important because it can determine the excitation and charged state of both the incoming projectile and of the atoms (both projectiles and target atoms) emitted as a result of collisions. The probability of the resonant processes depends on the superposition of the atomic wave functions with the tail of the electron wave functions in the solid. For metals, this means that the atomic states that are preferentially populated are those which lie in energy close to the Fermi level. An incident ion can be neutralized through AN or plasmon-assisted processes, or through resonant neutralization followed by AD decay. The first channel is dominant for high values of the work function, while the second dominates for low values of the work function. It is important to note that resonant processes depend on the local value of the work function, rather than on the macroscopic value. In fact, the presence of impurities, such as atoms adsorbed on the surface, alters the local value of the work function. At the adsorption sites, the incident ions can undergo neutralization mechanisms different from those that occur at the sites where there are atoms of the sample substrate. This makes Ion Neutralization Spectroscopy (INS) and Metastable Deexcitation Spectroscopy (MDS) an extremely sensitive surface structure analysis tool [1,33].

2.2. KEE

In kinetic electron emission (KEE), electrons are excited by the transfer of the kinetic energy carried by incoming projectiles. There are several mechanisms responsible for KEE in the interaction of slow singly charged ions with surfaces, some of which not yet understood. The first mechanism responsible for KEE is the binary collision of "free" valence electrons of the targets with the screened Coulomb field of the projectile. The maximum energy transfer to an electron occurs during head-on collisions, where the electron gains twice the projectile velocity after a single scattering. Therefore, energy and momentum conservation determine the threshold impact energy for this process. This corresponds to velocities in the range 1.5–3 $\times$ 10^7 cm s^{-1} (117–470 eV amu^{-1}) for most metals [6,34]. This mechanism is therefore the dominant excitation mechanism for light projectiles (H, He, Li) on metals, since binary collisions between the incoming atomic particles with nearly free electrons cannot transfer a large energy because of the large mass difference between the collisional partners.
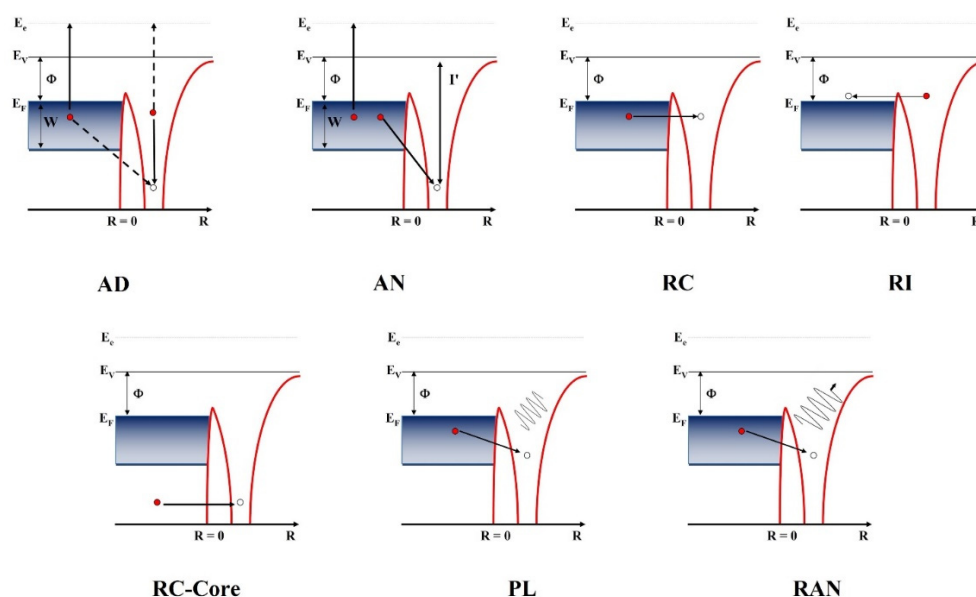
Figure 1. One-electron and two-electron transition that occurs for ions and excited atoms close to a solid surface. AD, Auger Deexcitation; AN, Auger Neutralization; RC, Resonant Capture; RI, Resonant Ionization; RC-Core, Resonant Capture from core level; PL, Plasmon Assisted Neutralization; RAN, Radiative Neutralization. In the figures, R is the distance from the surface, W is the width of the band, E_v and E_F are the vacuum and Fermi level, respectively, Φ is the metal work function, and E_e is the energy of the electron emitted in vacuum.

At impact energies below this threshold, electron emission is determined by the Molecular Orbital (MO) electron promotion mechanism [13,14]. The process occurs because of electron–electron interactions during the interpenetration of the electron clouds of the projectile and one of the target atoms, which are described as a transient molecule. Because the collision is a non-adiabatic process, some molecular levels increase their energy and electrons can be promoted to higher energies at the adiabatically-forbidden crossing between MOs. Excitations result when electrons are promoted directly into the ionization continuum or through autoionizing states [35–38]. Electron promotion processes are also characterized by well-defined thresholds, that depend on the combination of collision partners and can be experimentally determined and theoretically estimated from Molecular Orbital (MO) correlation diagrams. Studies of the dependence of KEE on impact parameter demonstrated the importance of electron promotion in the case of 4 keV Ar^+ impact on Ni surfaces [39].

Below the threshold for electron promotion, electron emission is non-vanishing, implying the existence of other sub-threshold processes. These processes have been poorly investigated. Experimental studies of electron emission in the interaction of singly charged ions with metal surfaces at normal or near normal incidence [40,41] showed that electron emission yields decrease exponentially with the reciprocal of projectile velocity. Some theoretical interpretations of these observations, in terms of either non-adiabatic one electron excitations or many-electron interactions [40,41], have been reported, but no definitive conclusion can be drawn from these studies.

3. Experiments

The experiments reported in this work have been conducted in UHV with a base pressure in the low 10^{-10} Torr range. Noble gas ions were produced by electron impact in a source operated at low discharge voltage to prevent significant formation of doubly charged species [42]. Na^+ ions were produced using a Kimball Physics ion gun. The current of the ion beams was of the order of 10^{-9} A, as measured with a faraday cup in the sample

position that also showed the Gaussian spatial distribution of the beams in both horizontal and vertical directions.

Energy distributions of emitted electrons were measured using two spectrometers. A fixed hemispherical energy analyzer situated at 60° from the beam direction and a hemispherical analyzer mounted on a rotatable goniometer. These analyzers had semi-acceptance angles of 25° and 1.5° and were operated at a constant pass-energy (ΔE = 40 and 50 eV, respectively). The spectrometers, the ion beams, and the surface normal were coplanar.

The polycrystalline Al samples (purity 99.999%) were cleaned by sputtering with 6 keV Ar^+ or Ne^+ ions. The cleanness of the sample was routinely checked by looking for the absence in ion- and electron-induced Auger spectra of oxygen and carbon contaminants.

Experimental Results

The upper panel of Figure 2 shows representative electron energy spectra $N€$ obtained with the fixed analyzer (angle integrated) from an Al surface under the impact of 100 eV He^+, Ne^+, and Ar^+ ions. The lower panel of Figure 2 reports the derivative dN/dE. The incident ion beams impinged on the surface at an incidence angle Θ_i = 80° (measured with respect to the surface normal). The $N(E)$ values are normalized to the beam current measured on the sample under positive bias. The spectra show characteristic features of AN. In the Auger Neutralization process, the maximum energy E_b of emitted electrons is $E_b = I' - 2\Phi$ [43], where I' is the ionization potential of the parent atom shifted by the image interaction and Φ is the metal work function. This energy corresponds to the case where both electrons participating in the Auger process are at the Fermi level.

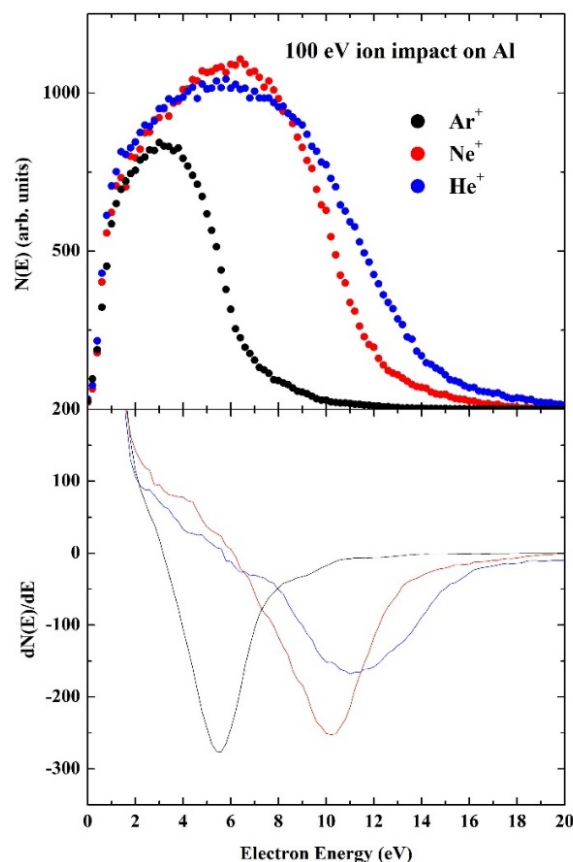**Figure 2.** Top: Energy spectra N(E) acquired with the large angle spectrometer for 100 eV He^+, Ne^+ and Ar^+ ions at Al surface. The incidence angle was Θ_I = 80°. Bottom: derivatives dN(E)/dE.

Therefore, the spectra show a high energy edge that depends on the ionization potential of the projectiles, which is broadened because of the velocity normal to the surface

of the ion [8]. In addition to the AN edge, a prominent shoulder that does not depend on the ionization potential of the projectiles is observed for He$^+$ and Ne$^+$ ions and attributed to plasmon excitation and decay [9–11]. Plasmon structures are usually visualized in the derivative of the spectra, $dN(E)/dE$, with minima at energies $E_m = E_{pl} - \Phi$. The derivatives of the spectra in the lower panel of Figure 2 for He and Ne projectiles show a shoulder that results in the minimum at about 10.5 eV. This energy is lower than the energy of the q = 0 Al bulk plasmon (15.5 eV minus Φ = 4.3 eV for Al). Angular studies of PEE [11] showed that the plasmons are excited at or above the surface, consistent with the idea of excitation by a shake-up due to the sudden disappearance of the dipole formed by the ion and its image charge [9] when incoming ions are neutralized by electron capture. This energy value suggests that the structure is more likely due to electron emission from decay of multipole surface plasmons excited at or above the surface [11,32] by potential energy transfer upon neutralization of the incoming ions. Meanwhile, Ar$^+$ neutralization on Al proceeds via the usual Auger process and is not mediated by plasmon excitation because of the lower energies released when incoming Ar$^+$ ions are neutralized; this is not sufficient to excite the plasmon.

The transition from the PEE regime to KEE is shown in Figures 3 and 4, reporting spectra for Ne and Ar ions on Al. The left panel of Figure 3 shows the spectrum N(E) of the electrons emitted by the Al surface bombarded by 1 keV Ar$^+$ ions at an incidence angle $\Theta_i = 60°$ and an observation angle $\Theta_e = 0°$. The spectrum is compared with that induced by Ne$^+$ ions at the same energy and the same geometry. The spectra have been normalized to the beams' current and width. At this ion energy, electron emission is dominated by PEE, but the spectra also show evidence of the onset of kinetic emission, as shown by the peak at a low energy of a few eV due to the cascade of secondary electrons and the two autoionization lines of Neon (Ne-I and Ne-II). These last features are due to the decay of projectiles scattered in vacuum after being excited in the triplet Ne**[$2p^4(^3P)3s^2$] and singlet Ne**[$2p^4(^1D)3s^2$] states during a binary collision with a target atom [35,36]. The area of the energy distributions, i.e., the electron emission yields, is therefore determined by the superposition of both potential and kinetic emission mechanisms. The latter increases its contribution, as shown in the right panel of Figure 3, reporting the spectra for 6 keV impact energy, which are dominated by KEE. In this emission regime, the line-shapes of the spectra for the two projectiles are very similar and characterized by the low energy peak followed by a monotonously decreasing background of cascade electrons. In the 10–15 eV range, the spectra reveal a broad feature due to electron emission from decay of bulk plasmons [11]. Bulk plasmon excitation is an indirect effect of electron promotion, as plasmons are excited by fast electrons travelling inside the solid (primarily Auger electrons from decay of 2p holes in Al), produced in binary symmetric collisions between two target atoms, recoiling in the atomic collision cascade initiated by incoming projectiles [17,32,38,44].
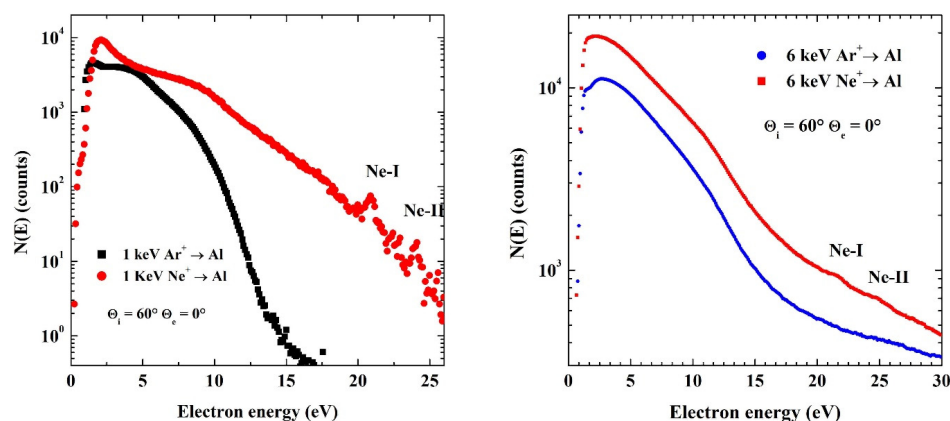

Figure 3. Energy spectra N(E) of electrons emitted from an Al surface by 1 keV (**left**) and 6 keV (**right**) Ne$^+$ and Ar$^+$ ions for an incident angle of 60° and observation angle 0° (spectra acquired with the angle resolved spectrometer).
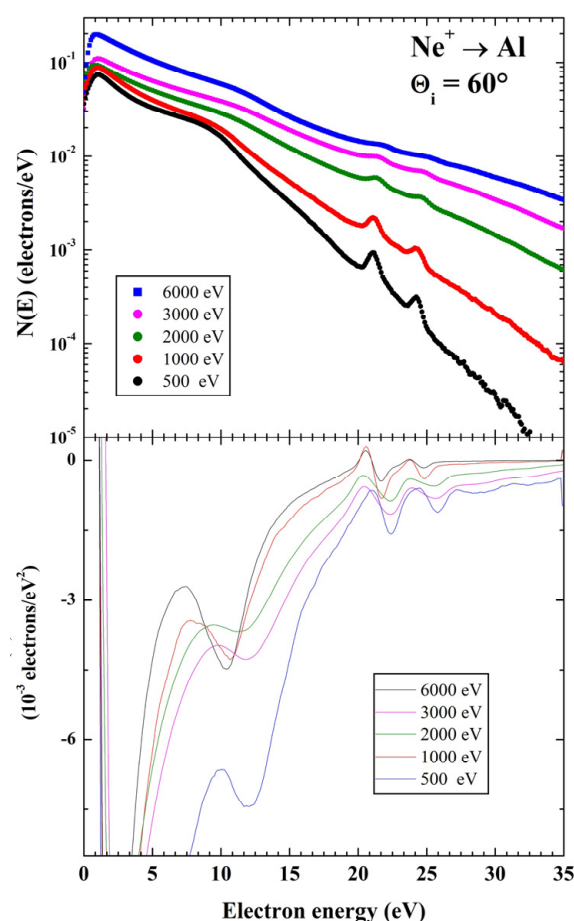
Figure 4. (**Top**): energy spectra N(E) of electrons emitted from an Al surface by Ne$^+$ ions as a function of ion incident energy. The spectra have been acquired with the large acceptance angle spectrometer for an incident angle of 60°. The spectra have been normalized to the total electron emission yields. (**Bottom**): derivative of the spectra that improve the visualization of the plasmon feature, showing the transition from potential excitation of surface plasmons to bulk plasmons excitations.

The transition from surface to bulk plasmon excitation is evidenced in Figure 4, which reports the spectra and their derivatives excited under Ne$^+$ impact. At the lowest incident energy of 500 eV used in the experiments shown in Figure 4, the derivative show minima at about 10.5 eV. As mentioned above, this value is lower than the energy of the q = 0 Al bulk plasmon and indicates that the structure is more likely due to electron emission from decay of multipole surface plasmons excited at or above the surface by potential energy transfer. At the highest incident energy of 6 keV, the observed plasmon structure appears at an energy closely corresponding to that of the q = 0 Al bulk plasmon, consistent with previous observations [11,32]. The spectra acquired at intermediate energies show that the structure due to bulk plasmon decay grows on the high energy side of the surface plasmon decay structure, as investigated in detail in [32].

Figure 5 reports energy distributions of electrons emitted from an Al surface bombarded by Na$^+$ ions at varying energies, with an incident angle $\Theta_i = 45°$ and an observation angle $\Theta_e = 0°$. Because of their low ionization potential, alkali ions cannot give rise to PEE and the spectra are characteristic of the KEE regime. The structure in the 10–15 eV energy range is due to electron emission from bulk plasmon decay, as evidenced in the derivative of the spectra in Figure 6, showing a minimum at the corresponding energy.
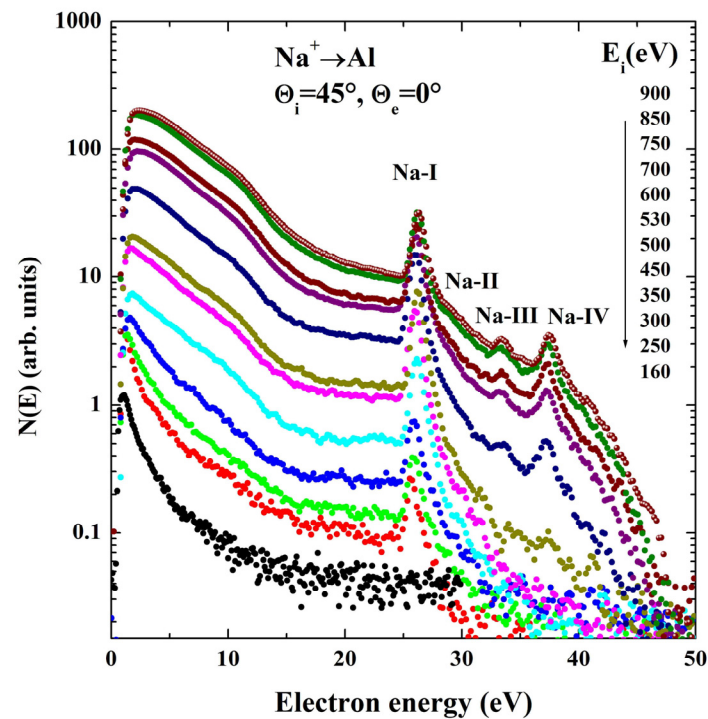
Figure 5. Energy spectra of electrons emitted from the Al surfaces under the impact of Na$^+$ ions at varying the energy of incoming ions, for fixed incidence and observation angles.
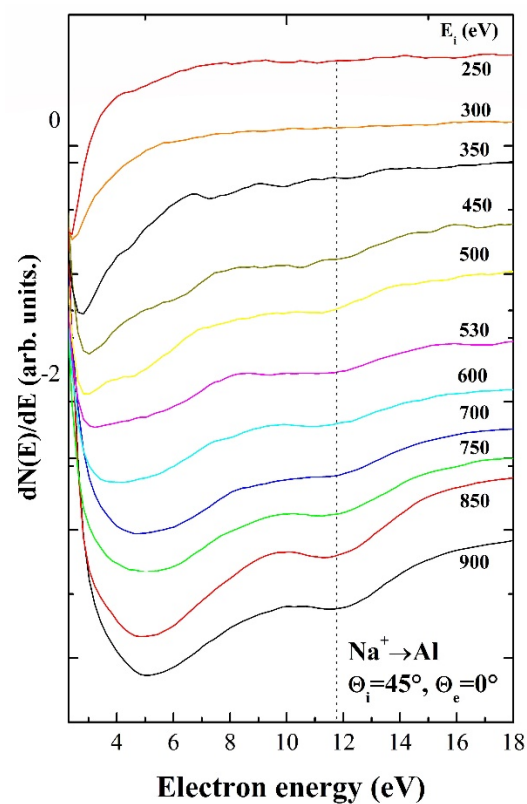

Figure 6. Derivatives of the spectra in Figure 5 that show the bulk plasmon dip.

The spectra for sodium and Neon projectiles in Figures 4 and 5 are also characterized by a series of narrow peaks in the 20–45 eV energy range. These peaks are known to originate from the Auger decay in vacuum of projectiles that have been scattered in vacuum with vacancies in the 2p shell, created by electron promotion in a binary collision with Al target

atoms. In the case of Neon, the spectra show two primary features, labelled Ne-I and Ne-II, due, respectively, to the decay of a triplet $[2p^4(^3P)3s^2]$ and a singlet $[2p^4(^1D)3s^2]$ state [35–37]. These peaks are followed by much weaker peaks due to the decay of $2p^3$ triply excited states of Neon projectiles [36,37]. These features are better visualized in the derivatives of the spectra in the lower panel of Figure 4 as small oscillations on the high energy side of the main peaks Na-I and Na-II.

Electron promotion processes show well defined thresholds, as shown in Figure 5 for sodium projectiles. For sodium, the peaks labelled from Na-I to Na-IV are observed. Peaks Na-I and Na-II are due to the decay of the $2p^53s^2$ and $2p^53s3p$ singly excited states of neutral sodium atoms, respectively, and appear at impact energies above a threshold of about 200 eV. Peaks Na-III and Na-IV originate from the decay of singly charged Na$^+$ ions, doubly excited in the $2p^4(^1D)3s^2$ and $2p^43s3p$ states, respectively, and are observed at impact energies higher than a threshold of about 500 eV [38].

At impact energy below the threshold of about 200 eV for the onset of promotion processes, the spectra of Figure 5 for Na projectiles show that electron emission does not vanish. As mentioned above, this range of impact energies has been poorly investigated and the underlying mechanism is still largely not understood [17,38,40,41].

The spectra in Figure 7, for 7 keV Kr$^+$ on Al and for 1 keV Na$^+$, have been extended to reveal electrons emitted up to a kinetic energy of 80 eV. In the 55–70 eV energy range, the spectra show features due to the Auger decay of 2p excited Al target atoms. Superimposed to the continuous background of secondary electrons, the Auger spectra of Aluminum reveal two contributions: the first consists of narrow lines, listed in ref. [45,46], due to LMM transitions in Al atoms sputtered in vacuum; the second is due to the LVV Auger decay of atoms in the solid matrix and involves valence electrons, and is therefore similar to the spectrum revealed under electron impact [47].
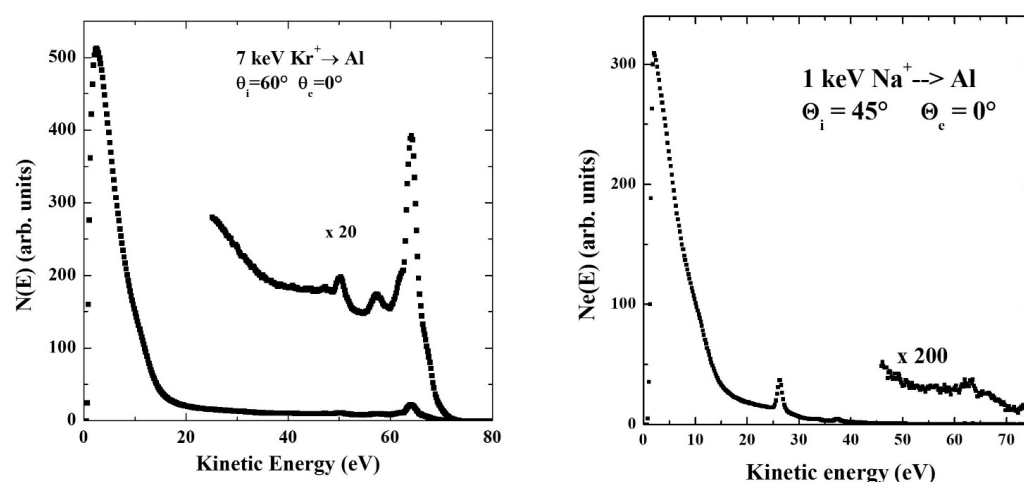

Figure 7. Spectra for 7 keV Kr$^+$ on Al (**left**) and for 1 keV Na$^+$ (**right**), extended to reveal the features due to the Auger decay of 2p excited Al target atoms In the 55–70 eV.

In the following section, the mechanism of electron promotion that produces excitation in both projectiles and target atoms will be discussed, because electronic excitation during binary atomic collisions in solids have received interest in the last few years due to their role in determining the energy loss of heavy projectiles in solids and the charge states of projectiles scattered at surfaces [18–31].

4. Electron Promotion

4.1. Correlation Diagrams

Electronic excitation during binary atomic collisions have been successfully described by a molecular orbital (MO) electron promotion model [13,14]. The model considers that a transient molecule is formed during the collision. The MOs of the collision system can be

considered to evolve adiabatically with the decrease in the internuclear distance only if the relative velocity of the nuclei is very small compared to the orbital velocity of the electrons. The intrinsic non-adiabaticity of the collision manifests in electronic excitations produced in one or both the colliding atoms so that, after the collision, they can have inner shell vacancies. These excitations are revealed when they decay via photon or Auger electron emission [35–38].

Fano and Lichten [13] first proposed that, under non-adiabatic conditions, the non-intersection rule between MOs could be no longer valid, so that electrons could be transferred from a MO to another at the adiabatically-forbidden crossings between these MOs (electron promotion). The excitations can be therefore described by the promotion of electrons in a sequence of crossings that occur in very narrow ranges of internuclear distances, so that the processes can be considered nearly vertical and characterized by well-defined thresholds. The thresholds can be determined experimentally as shown in Figure 5 and estimated through MO correlation diagrams [14,38,48]. For example, Figure 8 shows a correlation diagram calculated for the collisional systems Na-Al and Na$^+$-Al that explain the observed 2p excitations in sodium [38].
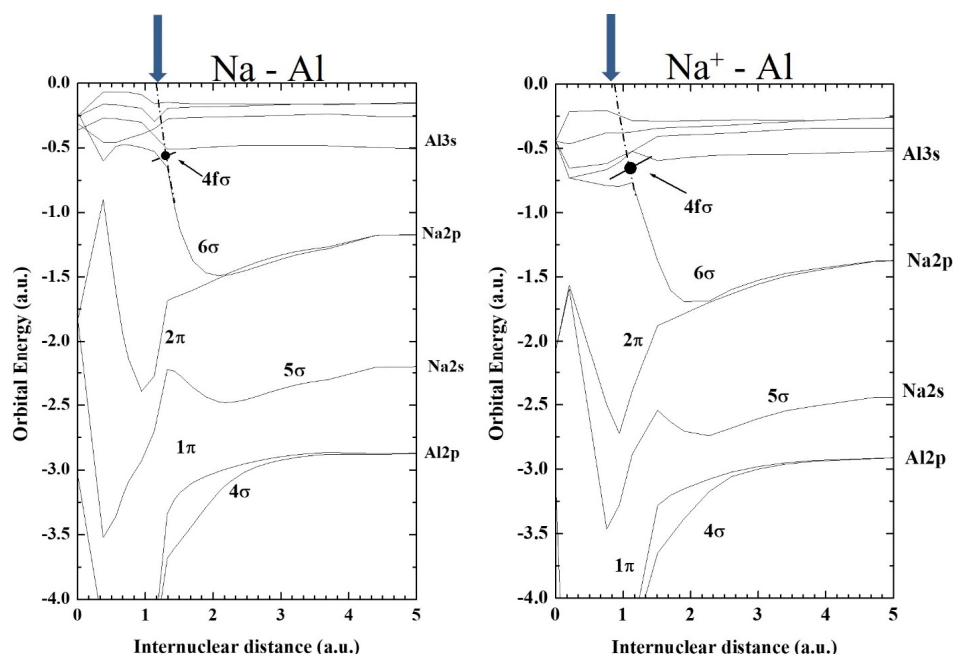

Figure 8. Adiabatic molecular-orbital (MO) correlation diagrams for the selected orbitals of Na-Al (**left**) and Na$^+$-Al (**right**), as calculated by the DFT method [38]. The dashed-dotted heavy curve indicates the evolution of diabatic level up to the continuum. The arrows on top approximately indicate the threshold for promotion of the electrons in the 4fσ MO.

These diagrams were calculated in [38] using the DFT method in the B3LYP formulation [49,50] using the computer code Gaussian 03 [51]. The diagram is calculated point by point, i.e., adiabatically. The diagram therefore describes the evolution with internuclear distance of the adiabatic MOs of the transient molecule, from the separated atom limits to the united atom limit at zero internuclear distance. To explain the observed electronic excitations, Fano and Lichten proposed to allow for electronic transitions at the adiabatically forbidden crossings between MOs. The diabatic path can therefore be constructed from the adiabatic correlation diagram as indicated by the dashed lines in Figure 8. This shows the well-known increase in the 4fσ MO correlated to the projectile's 2p level in the separate atom limit. We observe that, for binary collisions of neutral Na with an Al atom, the first forbidden crossing occurs at about 1.3 a.u., while the promotion path in the case of Na$^+$-Al is shifted to lower internuclear distances. Similar correlation diagrams have been reported for Neon projectiles [48].

The identification of the electron promotion processes can also be performed with the aid of qualitative correlation diagrams as with the one in Figure 9, constructed with rules given by Barat and Lichten [14]. This qualitative diagram does not show the evolution of the MOs with internuclear distance and does not give an indication on the thresholds for promotion. The rules given by Barat and Lichten establish correlation between the limits of separated atoms (R = ∞) and united atoms (R = 0), allowing for the individuation of specific promotion processes. The reported diagram is suited for the asymmetric systems Ar-Si and the Ne-Si, Ne-Al systems. In Figure 9, one individuates immediately the promotion of electrons in the 4fσ MO, correlated to the 2p level of the lighter collision partner.
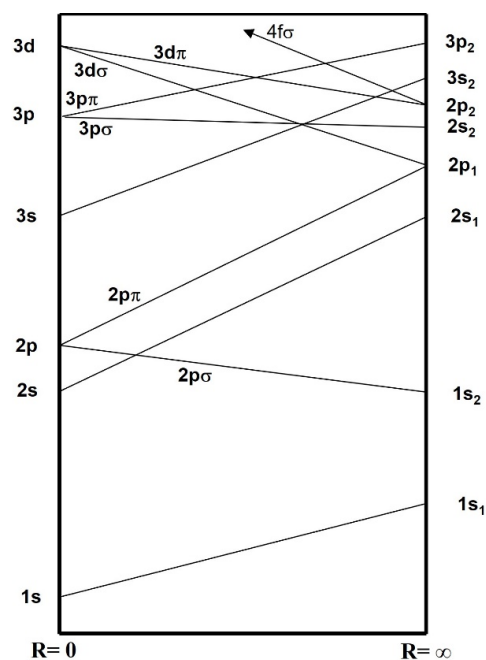

Figure 9. Qualitative correlation diagram constructed according to rules given in ref. [14], for collisions between two atoms of atomic number Z_1 and Z_2, with Z_1 slightly larger than Z_2.

The diagram also shows that other promotion processes are possible. 2s excitation in the lighter partner of the collision is ascribed to the 3pσ-3pπ rotational coupling. This process requires a shorter internuclear distance than 4fσ promotion, consistent with the 2s excitation in Neon colliding with Al surfaces recently observed at impact energies above about 1 keV [23,24].

Figure 9 also shows the 2pσ-2pπ promotion channel. In this process, an electron in the 2pσ MO can be promoted in the 2pπ, provided that there is a hole in this level correlated to the 2p level of Al [45,52]. While this channel is normally closed because the 2p level of targets including Al or Si are fully occupied, the high atomic density of solid targets opens the possibility of having collision processes in which the incident ion has one or more inner-shell vacancies, produced in a preceding collision.

4.2. 2p Excitation in Neon and Sodium Projectiles

The narrow discrete peaks in the 20–45 eV electron energy range observed for Sodium and Neon ions (projectiles lighter than Al) are due to the autoionization in vacuum of projectiles, scattered after being excited in the 2p level by electron promotion during binary atomic collisions with Al atoms [35–38]. The 2p excitation in projectiles lighter than Al is predicted by the molecular orbital electron promotion model, as shown in the correlation diagram in Figures 8 and 9. The spectra excited by Neon are dominated by two prominent features due to the decay of a triplet $[2p^4(^3P)3s^2]$ and a singlet $[2p^4(^1D)3s^2]$ state, respectively. As mentioned above, weaker peaks due to the decay of $2p^3$ triply excited states of Neon projectiles are observed at higher electron energies [36,37].

Similar observations are reported for sodium ions. The peaks of Na-I and Na-II are due to the decay of the $2p^5 3s^2$ and $2p^5 3s 3p$ singly excited states of neutral sodium atoms, respectively. The decay of the $2p^4(^1D)3s^2$ and $2p^4 3s 3p$ doubly excited states of Na^+ ions give rise to the peaks labelled Na-III and Na-IV [38]. An immediate consequence of this observation is that the Auger decay of these states results in different charge states for scattered projectiles. For Sodium, the Auger decay of the $2p^5$ states results in singly charged scattered ions. Therefore, these ions determine the anomalous charge fractions recently measured in experiments of sodium scattering at Al surfaces [21,22]. On the other hand, the observation of the Na-III and Na-IV features reveal the presence of doubly charged species in the scattered projectiles, which have not been investigated in charge fraction measurements. The observation of the decay of both $2p^4$ and $2p^3$ states leads to the same conclusions for Neon.

The formation of the 2p excited states is usually discussed according to a three-step model [35,36]. In the first step, charge exchange in the incoming trajectory results in efficient neutralization of the projectiles, and only a small percentage survive as an ion [35,37,53]. In the subsequent close approach to a target atom, 2p excitation occurs because of electron promotion in the transient quasi-molecule. In the third step, further non-local electron capture processes during their outgoing trajectory determine the final charge and excitation states of scattered particles. For Ne^+ projectiles, the neutralization of incoming ions can occur through a resonant, an Auger neutralization, or a plasmon-assisted process [12]. For incoming Na^+, only the resonant capture is operative because of the low ionization potential of the alkali atom [21]. The neutralization probabilities for all the possible processes are very high for slow ions and decrease with impact energy. Close to the surface, projectiles resonantly neutralized into excited states can be resonantly ionized again. Because of this complex sequence of charge transfer processes, in the energy range of interest, most of the Ne^+ and Na^+ atoms are neutralized to the ground state, while only a few percent survive as an ion. As shown in the correlation diagrams in Figure 8, the charge state of projectiles at the moment of the collision with a target atom exerts a strong influence on the 2p excitation. Collisions involving neutralized projectiles lead to the observation of the peaks Ne-I and Ne-II and Na-I and Na-II for neon and sodium, respectively. On the other hand, projectile ions that have survived neutralization lead to the doubly and triply excited states of Sodium and Neon, respectively. The excitation processes for neutrals and ions are observed at different energy thresholds, as shown in Figure 5 for sodium; this is consistent with the correlation diagrams in Figure 8. A threshold of 230 eV has been obtained in careful measurements for Neon [36]. A similar threshold is expected for neutral sodium, as observed in Figure 5. Actually, the expectation is somewhat lower. In fact, as a general property, the cross sections of electron promotion processes for a given element depend on the atomic number Z of the other collision partner [35,54], showing oscillations with maxima for the symmetric cases [55]. The doubly 2p excited peaks in sodium (and the triply excited peaks in neon [56]) are observed at impact energies above 500 eV (see Figure 5). Double 2p excitation in collisions involving Neon-like Na^+ ions are observed at a higher threshold energy because they require a smaller closest approach distance, due to the larger binding energy of the levels of Na^+ than those of Na^0, consistent with the molecular orbital correlation diagrams in Figure 8. The possibility mentioned previously [22], that the double 2p excitation in neutral sodium might require a shorter internuclear distances than one electron promotion, is excluded by the correlation diagrams in Figure 8. In fact, both single and double excitations are associated to the diabatic path of the correlated $4f\sigma$ molecular level and therefore occur with the same threshold.

The important implication of the foregoing discussion is that the double excitation for Neon and Neon-like Na^+ projectiles occurs simultaneously in a single scattering event and not by one electron promotion in two consecutive collisions, a long debated issue [57–62]. The dominance of the double promotion mechanism is consistent with the inelasticities Q_{bin} measured in single scattering experiments of Ne ions on Al and Si

as a function of the closest approach distance R_{min} [57,61]. In these experiments, Q_{bin} is observed to increase steadily as R_{min} decreases, starting from a threshold of about 0.7–0.8 Å, until saturation behavior occurs for both targets for R_{min} around 0.5 Å. For both targets, the values of Q_{bin} in the saturation region correspond to the 45 eV loss needed to form the doubly excited autoionizing states of Ne in the hard collision from a projectiles that has been neutralized on the incoming path. Evidence for direct ionization of Ne^0 to Ne^+ ($Q_{bin} \sim 20$ eV), expected in the one electron excitation and reionization model [59,60], have not been observed [58].

The basic assumption of the one electron promotion and reionization model is that, for collisions in a solid environment, electrons are promoted into the empty conduction band states of the solid and, after the collision, they are not localized into specific atomic orbitals [59,60], as with collisions in the gas phase. This band effect is generally referred to as (re)ionization, because most of the projectiles are neutralized during the approach to the surface. The model, however, is not consistent with the observation that, at impact energies below 500 eV, double excitations are revealed for neon but not for sodium. As previously discussed [15], given the occupancy of a 3 s electron in neutral sodium, the formation of doubly $2p$-excited states would require one or both promoted $2p$ electrons to be transferred to the solid. For example, the $2p^4(^1D)3s^2$ could be produced by the promotion of one electron into the empty $3s$ level while the second electron should be transferred into the conduction band. This process would therefore lead to the observation of the Na-III peak, with the same threshold as the Na-I and Na-II peaks, in contrast with our observation, as shown in Figure 5. This leads to the conclusion that reionization into the empty conduction states is not an important process.

The dominance of the single scattering regime is revealed by the changes in the line-shape of the autoionization lines with the scattering geometry and energy [23,24]. An example is reported in Figure 10, that shows angle resolved spectra, revealed to observe the variation of the line-shapes of the Neon features with the observation angle, for an incident ion energy $E_0 = 1$ keV and for an incidence angle $\Theta_i = 80°$. The spectra are shown normalized to the beam current and width. The spectral features in Figure 3 appear to be significantly broadening and shifting to higher energy as the observation direction is moved from the surface normal to 80°. This is due to the motion of the emitting atoms, so that, in the laboratory frame, the energy of emitted electrons will be revealed to be *Doppler* shifted [23,24] with respect to the value expected for a frame in which the emitting atom is at rest (20.35 eV for triplet and 23.55 eV for singlet). Figure 3 shows that the peak energy increases as Θ_e is changed from 0° to 80°. The shift toward higher energies of the peaks reveals that components of velocity in the direction of observation of the emitting neon are, on average, increasing with Θ_e. This is a consequence of two body scattering, in which the velocity of the scattered atoms increases as the scattering angles are decreased. The observation provides evidence of the dominance of the single scattering regimes and is consistent with earlier observation and simulations [37].

The spectra become also increasingly asymmetric, broadening on the low energy side. The asymmetric broadening is due to electrons emitted by excited Neon atoms scattered with lower components of velocity in the observation direction. These low components of velocity in the observation directions reveals the contribution to the emission of projectiles that have been more severely scattered, such as those excited in subsurface and multiple collisions. This conclusion is corroborated by measurements as a function of the observation and the incidence angles [23,24], which showed similar shift and broadening for both neon and sodium projectiles. Thus, the shift and the asymmetric broadening of the autoionization peaks are determined by the angular and energy distributions of excited scattered projectiles. The shift of the peaks reflects the kinematic properties of two-body scattering, allowing us to establish that double excitations in reflected projectiles are efficiently produced in single scattering events. The effect of collisions that produce more severe scattering, such as those that occurs inside the solid during the collision cascade, results in excited projectiles

scattered with low energy, and is revealed in the asymmetric spectral broadening; These collisions are prevalent for near normal incidence [23].
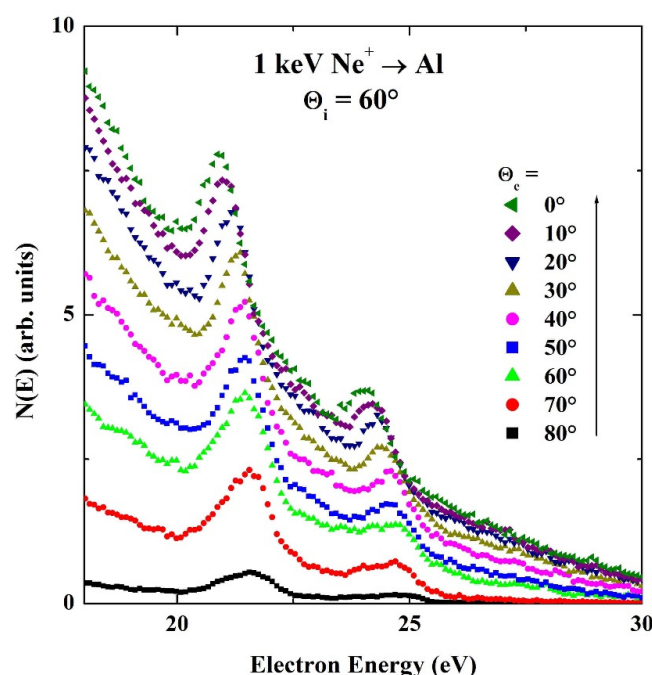

Figure 10. Ne I and Ne II autoionization spectra as a function of the observation angle Θ_e, for Ne$^+$ ions energy E_0 = 1 keV and at fixed incidence angle Θ_i = 60°.

4.3. 2p Excitation in Target Atoms

The discussion above revealed the importance of subsurface collisions in determining the line-shape of the autoionization lines of scattered projectiles. The Auger electron emission from the decay of 2p excitation of target atoms provides further insight into the electronic excitation and energy deposition mechanisms that occur inside the solid during the cascade of atomic collisions initiated by incoming projectiles. 2p excitations in the Al target atoms are reported in Figure 7 for the case of 7 keV Kr$^+$ and 1 keV Na$^+$ ion impact on Al. According to the electron promotion model, the probability of 2p excitation in Al via 4fσ promotion in collision with heavier projectiles like krypton and Argon is low because of the large mass difference between the two colliding partners. For lighter projectiles like sodium and neon, the probability for 2p excitation in Al via the rotational coupling of the 3dσ-3dπ-3dδ MOs (predicted by the correlation diagram in Figure 9) is also low and becomes sizeable at higher energies because it requires short internuclear distances [63]. On the other hand, the promotion of electrons in the 4fσ MO in symmetric collision between two recoiling Al atoms can efficiently produce 2p excitation in the target atoms and at lower thresholds. The dominance of symmetric Al-Al collisions has been demonstrated by observing that the Auger intensities have the same threshold for several projectiles when plotted as a function of γE_0, the maximum energy transferred in a projectile- target (P-T) collision [64], where E_0 is the incident ion energy and $\gamma = 4m_1m_2/(m_1+m_2)^2$. The energy γE_0 is therefore the minimum energy that must be transferred to an Al atom to produce the 2p excitation in a subsequent symmetric collision with another target atom.

Experiments also reveal an additional process that can produce 2p excitation in Al in asymmetric collisions with lighter elements [56]. This process has been individuated at impact energies below the threshold for excitation in symmetric collision. For sodium projectiles [38], the LMM Auger spectrum of Al is observed at impact energies lower than the threshold energy for excitation in target Al-Al symmetric collisions (~900 eV [64]) and very similar to the threshold for the observation of the Na III and Na-IV peaks. This indicates the occurrence of a vacancy transfer process that produces the 2p excitation in Al during an asymmetric collision with a Na$^+$. This vacancy transfer process has been

ascribed to a dielectronic transitions, in which an outer electron recombines one of the two $4f\sigma$ vacancies, releasing energy to an electron in the $3d\sigma$ or the $2p\pi$ MOs correlated to the 2p level of Al. This process of autoexcitation was first identified for the Ar-Si [65] and for Ne-Al systems [56] and, recently, in the interaction of He ions with Aluminum [16,64]. In the case of Helium projectiles, the process is associated with the promotion of both the electrons in the $3d\sigma$ MO, correlated to the 1s level of Helium.

5. Solid Target Effects

The molecular orbital electron promotion model has been developed for collisions in the gas phase, but it also satisfactorily describes collisions that occur in solids. The solid environment, however, is not merely a spectator, but introduces effects; this means that the Auger spectra can be substantially different from those revealed in the gas phase. A first immediate example of these solid target effects is the observation of the LVV component in the Auger spectra of Al target atoms due to atoms decaying in the solid.

The solid environment can also be important in the excitation process. Evidence comes from the strong emission from the triplet state that gives origin to the Ne-I peak. In fact, the promotion model predicts the excitation of the $4f\sigma$ electrons, which cannot lead to the excitation of a triplet ^{3}P state. In fact, the triplet peak results are very weak in the gas phase, where only a few percent of collisions lead to its excitation [35,66]. It has been shown that the triplet state can be excited by an Auger rearrangement process that occurs during the collision. In this mechanism, an electron from a Rydberg orbital fills one of the two holes in the $4f\sigma$ MO, while an electron in the $3d\pi$ state is excited to a higher lying state. The low probability of the process explains the weak intensity of the Ne-I peak in the gas phase [66]. However, this process can be favored for collision in the solid phase because of the large number of available valence and conduction electrons [31,35]. This issue has been recently discussed by our group, showing that the conversion results are very sensitive to the electronic structure at the excitation site [31]. This is consistent with the idea that the singlet to triplet conversion occurs during the collision, while the two atoms are still coupled in a molecular state, as required for the occurrence of an Auger rearrangement process. In turn, the conversion provides further evidence that the double 2p excitation is produced through simultaneous promotion of both $4f\sigma$ electrons in a single scattering event. Moreover, in the reionization model, the triplet state can be created only during a collision involving a Ne$^+$ atom that survived surface neutralization with a hole originally present in the 2p level correlated to the $3d\pi$ MO, meaning that the promotion of one $4f\sigma$ electron leads to the triplet configuration. This implies that collisions involving neutral projectiles should not lead to the triplet configuration, which is not consistent with an experimental observation that revealed a very similar singlet to triplet intensity ratio for the impact of both Ne$^+$ ions and Ne^0 neutrals [35].

The physical picture of the singlet to triplet conversion that emerges from our study is that of an electron correlation effect that occur on a sub-femtosecond time scale while the colliding atoms are still coupled in the quasi-molecular system [65]. The dielectronic autoexcitation discussed above is another electron correlation effect that can have an important effect, as it can produce a $2p\pi$ vacancy in the lighter collision partner. This process can therefore open the $2p\sigma$-$2p\pi$ promotion channel. In this process, an electron in the $2p\sigma$ MO can be promoted in the $2p\pi$, provided that there is a hole in this level, correlated to the 2p level of Al [54], as shown by the correlation diagram in Figure 9. While this channel is normally closed because the 2p level of targets such as Al are fully occupied, the high atomic density of solid targets opens the possibility of having collision processes in which the incident ion has one or more inner-shell vacancies, produced in a preceding collision. Therefore, the $2p\sigma$-$2p\pi$ process results in holes in the correlated atomic 1s level of the lighter collision partner, which have been identified at impact energies of tens and hundreds of keV by the characteristic K X-ray emission. For example, Ne K X-ray production has been reported for Ne projectiles incident on Mg, Al, Si, and P targets [52,54] at impact energies ranging from several tens to some hundreds keV. A sequence of these

collisional excitations in solids explains the large energy losses in the keV range, that have been revealed recently in experiments of heavy ions transmission through Si solid samples along channeled and random trajectories [18,19].

6. Electron Emission Intensities

The total electron emission yields γ_{tot} is reported in the upper panel of Figure 11 as a function of the ion incident energy for Neon and krypton projectiles incident with $\Theta_i = 60°$. The yields have been obtained from measurements of the currents measured on the sample under positive and negative bias. Yields measured in this work are displayed along with those by Neon and Krypton projectiles reported in earlier work [17,32]. As mentioned above, Al Auger electrons develop an electronic collision cascade in which plasmons and secondary electrons are excited [17,32,38,44]. The lower panel of Figure 11 reports the ratio $R = I_{HE}/I$ between the area I_{HE} of the region of the spectrum in the 40–75 eV energy range in Figure 3 and the area I of the spectrum of low energy electrons. As shown in Figure 3, the high energy portion of the spectrum is dominated by the Auger emission from Al atoms and we find that the dependence of I_{HE} on incident ion energy follows a trend similar to that reported for Al-Auger intensities obtained after subtraction of the background of secondary electrons [17,29,44]. We have also verified that the area I follows a trend closely resembling that of the emission yields γ_{tot} [17,29]. For comparison, Figure 11 also reports the yields and the ratio R for Kr projectiles [17] that show a similar behavior. The ratios R for the two projectiles show a similar threshold, slightly below 1 keV. Above the threshold, the ratios R increase approaching saturation values. The different increase in the ratios for different projectiles is ascribed to the different contribution to the total electron emission yields of potential electron emission, which is larger for Neon in view of its larger ionization potential.
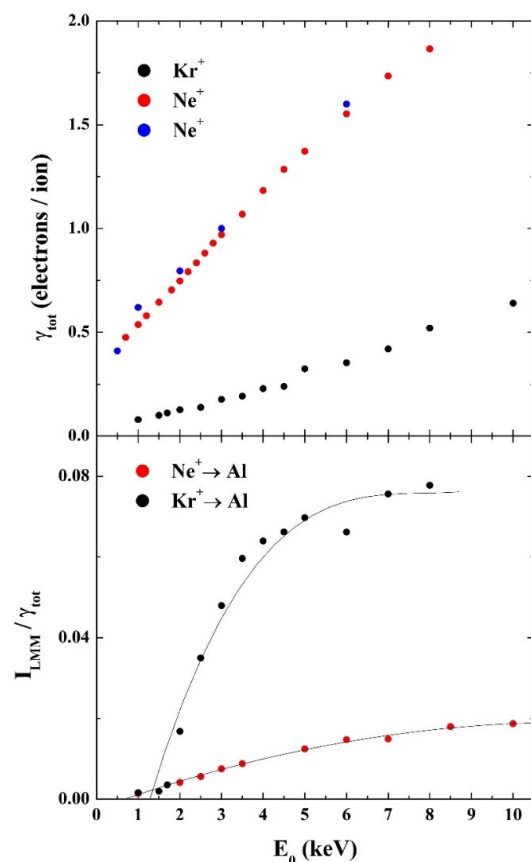

Figure 11. (**Top**): Electron emission yields γ_{tot} for Kr[+] [17] and Ne[+] impact on Al (blue circles are from this work, red circles are from [32]). (**Bottom**): The ratio R = I_{HE}/I for Kr[+] [17] and Ne[+] impact on Al. The lines through data points are to guide the eyes.

The observations in Figure 11 are therefore consistent with the conclusion that the total electron emission yield is determined by the electronic collision cascade initiated by energetic Auger electrons of Aluminum travelling inside the solid and resulting in the generation of secondary electrons and bulk plasmons [17,38,44].

7. Concluding Remarks

This work has been devoted to an experimental study by electron spectroscopy of charge exchange effects in the scattering of low energy singly charged heavy ions with atomically clean Al surface. The analysis of the energy distributions reveals the complex interplay of local and non-local interactions during the scattering.

Autoionization spectra of 2p excited states of Neon and Sodium scattered projectiles give insight into the dynamics of the scattering of the projectiles. The shift and the broadening of the autoionization lines due to the motion of the emitting atoms in vacuum show that the double 2p excitation in Neon projectiles occurs simultaneously in a single scattering event and not in two consecutive collisions, as commonly assumed.

The decay of 2p holes in Al atoms, produced in symmetric collisions between two recoiling target atoms, is the driving mechanism of electron emission for projectiles ions incident with energies in the keV range.

The work highlights the importance of electron correlation effects that occur during atomic collision in solids. These effects are determined by the electron-electron interaction that result in two-electron transitions while the colliding atoms are still coupled in the molecular system. These effects explain the intense emission of the triplet state for Neon projectiles and the 2p excitation of Al target atoms at impact energies below the threshold for excitation in symmetric collisions. The investigations of these effects in atomic collisions and in ion-solid interactions have been quite sparse and our work evidences the importance of properly considering these effects in order to understand charge exchange and energy deposition processes.

It is interesting to note that studies of secondary electron emission in many applications usually focus on the total electron emission yields, an integral quantity which sum up the effects of all the involved excitation and emission processes. The combined analysis of energy distributions and electron emission yields presented here reveal the complex interplay of many excitation and emission phenomena that involve both solid state concepts like plasmons and a description of atomic collisions, thus stressing the wealth of information that can be provided by electron spectroscopy experiments.

Data Availability Statement: Data are available upon reasonable request.

Conflicts of Interest: The author declares no conflict of interest.

References

1. Vanselow, R.; Howe, R.F. (Eds.) *Chemistry and Physics of Solid Surfaces VII*; Springer: Berlin/Heidelberg, Germany, 1988; p. 341.
2. Hagstrum, H.D. Theory of Auger Ejection of Electrons from Metals by Ions. *Phys. Rev.* **1954**, *96*, 336. [CrossRef]
3. Hagstrum, H.D. Ion-Neutralization Spectroscopy of Solids and Solid Surfaces. *Phys. Rev.* **1966**, *150*, 495. [CrossRef]
4. Hagstrum, H.D.; Becker, G.E. The Interrelation of Physics and Mathematics in Ion-Neutralization Spectrosocpy. *Phys. Rev.* **1971**, *4*, 4187. [CrossRef]
5. Matsakis, D.; Coster, A.; Laster, B.; Sime, R. A renaming proposal: "The Auger-Meitner effect". *Phys. Today* **2019**, *72*, 9–10. [CrossRef]
6. Baragiola, R.A.; Riccardi, P. Electron Emission from Surfaces Induced by Slow Ions and Atoms. In *Reactive Sputter Deposition*; Depla, D., Mahieu, S., Eds.; Springer Series in Material Science; Springer: Berlin/Heidelberg, Germany, 2008; Volume 109, Chapter 2.
7. Baragiola, R.A. Electron Emission from Slow Ion-Solid Interactions. In *Low Energy Ion-Surface Interactions*; Rabalais, J.W., Ed.; Wile: New York, NY, USA, 1994; Chapter 4.
8. Monreal, R. Auger Neutralization and Ionization Processes for Charge Exchange between Slow Noble Gas Atoms and Solid Surfaces Prog. *Surf. Sci.* **2014**, *89*, 80. [CrossRef]

9.   Baragiola, R.A.; Dukes, C.A. Plasmon-Assisted Electron Emission from Al and Mg Surfaces by Slow Ions. *Phys. Rev. Lett.* **1996**, *76*, 2547. [CrossRef] [PubMed]

10.   Riccardi, P.; Baragiola, R.A.; Dukes, C.A. Electron Emission and Electronic Stopping in the Interaction of Slow Helium Ions with Aluminum. *Phys. Rev. B* **2015**, *92*, 045425. [CrossRef]

11.   Riccardi, P.; Barone, P.; Bonanno, A.; Oliva, A.; Baragiola, R.A. Angula Studies of Potential Electron Emission in the Interaction odf Slow Ions with Al Surfaces. *Phys. Rev. Lett.* **2000**, *84*, 378. [CrossRef] [PubMed]

12.   Baragiola, R.A.; Dukes, C.A.; Riccardi, P. Plasmon Excitation in Ion-Solid Interactions. *Nucl. Instrum. Methods B* **2001**, *182*, 73–83. [CrossRef]

13.   Fano, U.; Lichten, W. Interpretation of Ar^+- Ar Collisions at 50 keV. *Phys. Rev. Lett.* **1965**, *14*, 627.

14.   Barat, M.; Lichten, W. Extension of the Electron-Promotion Model to Asymmetric Atomic Collisions. *Phys. Rev. A* **1972**, *6*, 211. [CrossRef]

15.   Riccardi, P.; Cosimo, F.; Sindona, A. Absence of Reionization in Low Energy Na^+ scattering from Al Surfaces. *Phys. Rev. A* **2018**, *97*, 032703. [CrossRef]

16.   Riccardi, P.; Sindona, A.; Dukes, C.A. Evidence for Charge Exchange Effects in Electronic Excitations in Al by Slow singly charged He ions. *Nucl. Instrum. Methods B* **2016**, *382*, 7. [CrossRef]

17.   Commisso, M.; Minniti, M.; Sindona, A.; Bonanno, A.; Oliva, A.; Baragiola, R.; Riccardi, P. Kinetic Electron Excitation in the Interaction of Slow Kr^+ Ions with Al Surfaces. *Phys. Rev. B* **2005**, *72*, 165419. [CrossRef]

18.   Lohmann, S.; Holeňák, R.; Grande, P.; Primetzhofer, D. Trajectory Dependence of Electronic Energy-Loss straggling at keV Ion Energies. *Phys. Rev. B* **2023**, *107*, 085110. [CrossRef]

19.   Lohmann, S.; Holeňák, R.; Primetzhofer, D. Trajectory-Dependent Electronic Excitation by Light and Heavy Ions Around and Below the Bohr Velocity. *Phys. Rev. A* **2020**, *102*, 062803. [CrossRef]

20.   Lohmann, S.; Primetzhofer, D. Disparate Energy Scaling of Trajectory-Dependent Electronic Excitations for Slow Protons and He Ions. *Phys. Rev. Lett.* **2020**, *124*, 096601. [CrossRef]

21.   Liu, P.; Yin, L.; Zhang, Z.; Ding, B.; Shi, Y.; Li, Y.; Zhang, X.; Song, X.; Guo, Y.; Chen, L.; et al. Anomalous Neutralization Characteristics in Na^+Neutralization on Al(111) Surfaces. *Phys. Rev. A* **2020**, *101*, 032706. [CrossRef]

22.   Wei, M.; Wang, X.; Guo, X.; Liu, P.; Ding, B.; Shi, Y.; Song, X.; Wang, L.; Liu, X.; Yin, L.; et al. Low-Energy Na^+ Neutralization on Al(111) and Cu(110) Surfaces at Grazing Incidence. *Nucl. Instrum. Methods B* **2020**, *478*, 239–243. [CrossRef]

23.   Runco, D.; Riccardi, P. Single Versus Double 2p Excitation in Neon Projectiles Scattered from Surfaces. *Phys. Rev. A* **2021**, *104*, 042810. [CrossRef]

24.   Runco, D.; Riccardi, P. Collisional Excitation in Neon-like Projectiles Scattered from Al. *Solid State Commun.* **2021**, *340*, 114534. [CrossRef]

25.   Li, S.-M.; Mao, F.; Zhao, X.-D.; Li, B.-S.; Jin, W.-Q.; Zuo, W.-Q.; Wang, F.; Zhang, F.-S. First Principle Study of the Electronic Stopping Power of Indium for Protons and He Ions. *Phys. Rev. B* **2021**, *104*, 214104. [CrossRef]

26.   Runco, D. Charge and Excitation State of Na Projectiles Scattered from Al Surfaces. *Radiat. Eff. Defects Solids* **2021**, *176*, 995. [CrossRef]

27.   Holenak, R.; Lohman, S.; Sekula, F.; Primetzhofer, D. Simultaneous Assessment of Energy, Charge State and Angula Distribution for Medium Energy Ions Interacting with Ultra-Thin Self-Supporting Targets: A time-of-Flight Approach. *Vacuum* **2021**, *185*, 109988. [CrossRef]

28.   Ntemou, E.; Holeňák, R.; Primetzhofer, D. Energy Deposition by H and He Ions at keV Energies in Self-Supporting, Single Crystalline SiC Foils. *Radiat. Phys. Chem.* **2022**, *194*, 110033. [CrossRef]

29.   Riccardi, P.; Dukes, C.A. 2p Excitation in Target Atoms in the Interactionof Slow Ions with Al Surfaces. *Surf. Sci.* **2022**, *719*, 122025. [CrossRef]

30.   Riccardi, P.; Dukes, C.A. Effects of the Solid Target on Electronic Excitations During binary Atomic Collisions in the Interaction of Ne Ions with Al Surfaces. *Vacuum* **2022**, *204*, 111393. [CrossRef]

31.   Riccardi, P.; Dukes, C.A. Excitation of the Triplet $2p^4(^3P)3s^2$Autoionixing State of Neon by Molecular Orbital Electron Promotion at Solid Surfaces. *Chem. Phys. Lett.* **2022**, *798*, 139610. [CrossRef]

32.   Barone, P.; Bonanno, A.; Camarca, M.; Oliva, A.; Xu, F.; Riccardi, P.; Baragiola, R.A. The Excitation of Collective Electronic Modes in Al by Slow Singly Charged Ne Ions. *Surf. Sci.* **2001**, *480*, L420. [CrossRef]

33.   Karmakar, P.; Liu, G.F.; Sroubek, Z.; Yarmoff, J. Ion Beam Induced Formation and Interrogation of Au Nanoclusters. *Phys. Rev. Lett.* **2007**, *98*, 215502. [CrossRef]

34.   Winter, H.; Lederer, S.; Winter, H. Fermi Momentum Above Metal Surfaces from Electrons Ejected by Impact of He Ions. *Europhys. Lett.* **2006**, *75*, 964. [CrossRef]

35.   Zampieri, G.; Meier, F.; Baragiola, R.A. Formation of Autoionizing States of Ne in Collisions with Surfaces. *Phys. Rev. A* **1984**, *29*, 116. [CrossRef]

36.   Xu, F.; Mandarino, N.; Oliva, A.; Zoccali, P.; Camarca, M.; Bonanno, A.; Baragiola, R.A. Projectile $L_{2,3}$-Shell Electron Excitation in Slow Ne^+-Al Collisions. *Phys. Rev. A* **1994**, *50*, 4040. [CrossRef] [PubMed]

37.   Guillemot, L.; Lacombe, S.; Maazouz, M.; Tuan, V.N.; Esaulov, V.; Sanchez, E.; Bandurin, Y.; Daschenko, A.; Drobnich, V. Dynamics of Excited State Production in the Scattering of Inert Gas Atoms and Ions from Mg and Al Surfaces. *Surf. Sci.* **1996**, *365*, 353. [CrossRef]

38. Minniti, M.; Commisso, M.; Sindona, A.; Sicilia, E.; Bonanno, A.; Barone, P.; Baragiola, R.; Riccardi, P. Kinetic Electron Emission from Al Surfaces by Slow Ions. *Phys. Rev. B* **2007**, *75*, 045424. [CrossRef]
39. Rabalais, J.; Bu, H.; Roux, C. Impact-Parameter Dependence of Ar⁺-Induced Kinetic Electron Emission from Ni(110). *Phys. Rev. Lett.* **1992**, *69*, 1391. [CrossRef]
40. Lorincik, J.; Sroubek, Z.; Eder, H.; Aumayr, F.; Winter, H. Kinetic Electron Emission from Clean Polycrystalline Gold Induced by Impact of Slow C⁺, N⁺, O⁺, Ne⁺, Xe⁺, and Au⁺ Ions. *Phys. Rev. B* **2000**, *62*, 16116. [CrossRef]
41. Lederer, S.; Maass, K.; Blauth, D.; Winter, H.; Winter, H.P.; Aumayr, F. Kinetic Electron Emission from the Selvage of a Free-Electron-Gas Metal. *Phys. Rev. B* **2003**, *67*, 121405(R). [CrossRef]
42. Riccardi, P.; Sindona, A.; Dukes, C. Local Charge Exchange of He⁺ Ions at Aluminum Surfaces. *Phys. Lett. A* **2017**, *381*, 1174. [CrossRef]
43. Barone, P.; Sindona, A.; Baragiola, R.; Bonanno, A.; Oliva, A.; Riccardi, P. Sub-Threshold Plasmon Excitation in Free-Electron Metals by Helium Ions. *Nucl. Instrum. Methods B* **2003**, *209*, 68. [CrossRef]
44. Minniti, M.; Commisso, M.; Sindona, A.; Barone, P.; Bonanno, A.; Oliva, A.; Riccardi, P. The Role of Al-Auger Electrons in Kinetic Electron Emission from Al Surfaces by Slow Ne⁺ and Na⁺ Ions. *Nucl. Instrum. Methods B* **2007**, *257*, 618. [CrossRef]
45. Valeri, S. Auger Electron Emission by Ion Impact on Solid Surfaces. *Surf. Sci. Rep.* **1993**, *17*, 85. [CrossRef]
46. Baragiola, R.A.; Alonso, E.; Raiti, H. Ion-Induced Auger-Electron Emission from Aluminum. *Phys. Rev. A* **1984**, *25*, 1969. [CrossRef]
47. Baragiola, R.A. Principle and Mechanisms of Ion Induced Electron Emission. *Nucl. Instrum. Methods B* **1993**, *78*, 223. [CrossRef]
48. Lorincik, J.; Sroubek, Z. Non-Adiabatic Electron Excitation in Ion-Induced Kinetic Electron Emission from Metal Surfaces. *Nucl. Instrum. Methods B* **2000**, *164–165*, 633–640.
49. Becke, A.D. Density-Functional Thermochemistry. III. The Role of Exact Exchange. *J. Chem. Phys.* **1993**, *98*, 5648. [CrossRef]
50. Stephens, P.J.; Devlin, F.J.; Chabalowski, C.F.; Frisch, M.J. Ab Initio Calculations of Vibrational Absorption and Circular Dichroism Spectra Using Density Functional Force Fields. *J. Phys. Chem.* **1994**, *98*, 11623. [CrossRef]
51. Frisch, M.J.; Trucks, G.W.; Schlegel, H.B.; Scuseria, G.E.; Robb, M.A.; Cheeseman, J.R.; Montgomery, J.A., Jr.; Vreven, T.; Kudin, K.N.; Burant, J.C.; et al. *Gaussian 03, Revision A.1*; Gaussian Inc.: Pittsburgh, PA, USA, 2003.
52. Wille, U.; Hippler, R. Mechanisms of Inner-Shell Vacancy Production in Slow Ion-Atom Collisions. *Phys. Rep.* **1986**, *132*, 129–260. [CrossRef]
53. Beckschulte, M.; Taglauer, E. The Influence of Work Function Changes on the Charge Exchange in Low-Energy Ion Scattering. *Nucl. Instrum. Methods* **1993**, *78*, 29. [CrossRef]
54. Taulbjerg, K.; Fastrup, B.; Laegsgaard, E. Heavy-Ion-Induced X-ray Production in Solids. *Phys. Rev. A* **1973**, *8*, 1814. [CrossRef]
55. Saris, F.; Bierman, D.J. The Influence of Outer-Shell Excitation on the X-ray Production in Ion-Atom Collisions. *Phys. Lett. A* **1971**, *35*, 199. [CrossRef]
56. Xu, F.; Mandarino, N.; Oliva, A.; Zoccali, P.; Camarca, M.; Bonanno, A. Al Target 2p Electron Excitation in Asymmetric Collisions with Very Low Energy Ne⁺ Projectiles. *Nucl. Instrum. Methods B* **1994**, *90*, 564. [CrossRef]
57. Gordon, M.; Mace, J.; Giapis, K. Charge-Exchange Mechanisms at the Threshold for Inelasticity in Ne⁺ Collisions with Surfaces. *Phys. Rev. A* **2005**, *72*, 012904. [CrossRef]
58. Mace, J.; Gordon, M.J.; Giapis, K.P. Evidence of Simultaneous Double-Electron Promotion in F⁺ Collisions with Surfaces. *Phys. Rev. Lett.* **2006**, *97*, 257603. [CrossRef]
59. Souda, R.; Yamamoto, K.; Hayami, W.; Aizawa, T.; Ishizawa, Y. Band Effect on Inelastic Rare Gas Collisions with Solid Surfaces. *Phys. Rev. Lett.* **1995**, *75*, 3552. [CrossRef]
60. Souda, R.; Yamamoto, K.; Hayami, W.; Aizawa, T.; Ishizawa, U. Low-Energy He and Ne Scattering from Al(111): Reionization Versus Autoionization. *Surf. Sci.* **1996**, *363*, 139. [CrossRef]
61. Manicò, G.; Ascione, F.; Mandarino, N.; Bonanno, A.; Riccardi, P.; Alfano, P.; Zoccali, P.; Oliva, A.; Camarca, M.; Xu, F. Double 2p Electron Excitation in Low-Energy Ne⁺ Single Scattering from a Si Surface: An Energy Loss Study. *Surf. Sci.* **1997**, *392*, L7–L10. [CrossRef]
62. Xu, F.; Manico, G.; Ascione, F.; Bonanno, A.; Oliva, A.; Baragiola, R. Inelastic Energy Loss in Low-Energy Ne⁺ Scattering from a Si Surface. *Phys. Rev. A* **1998**, *57*, 1096. [CrossRef]
63. Schneider, D.; Nolte, G.; Wille, U.; Stolterfoht, N. Total Cross Sections for L-Shell Auger-Electron Production and Vacancy Production in Slow Ar-Si Collisions. *Phys. Rev. A* **1983**, *28*, 161. [CrossRef]
64. Riccardi, P.; Sindona, A.; Dukes, C. Double Electron Excitation in He Ions Interacting with an Aluminum Surface. *Phys. Rev. A* **2016**, *93*, 042710. [CrossRef]
65. Stolterfoht, N. Evidence for Autoexcitation producing Inner-Shell Vacancies in Slow Ion-Atom Collisions. *Phys. Rev. A* **1993**, *47*, R763. [CrossRef] [PubMed]
66. Østgaard-Olsen, J.; Andersen, T.; Barat, M.; Courbin-Gaussorgues, C.; Sidis, V.; Pommier, J.; Agusti, J.; Russek, A. Excitation and Charge Transfer in Low-Energy Na⁺-Ne Collisions. *Phys. Rev. A* **1979**, *19*, 1457. [CrossRef]